Rare Metal Materials and Engineering
Volume 53, Issue 12, December 2024
Available online at www.rmme.ac.cn

Science Press

Cite this article as: Yin Dongsong, Liu Zhiyuan, Zhang Youyou, et al. Effect of Compression Passes on Mechanical Properties and Corrosion Behavior of ZK60 Magnesium Alloy[J]. Rare Metal Materials and Engineering, 2024, 53(12): 3338-3347. DOI: 10.12442/j.issn.1002-185X.20240102.

ARTICLE

Effect of Compression Passes on Mechanical Properties and Corrosion Behavior of ZK60 Magnesium Alloy

Yin Dongsong[1], Liu Zhiyuan[2], Zhang Youyou[2], Mao Yong[2], Han Tianming[3]

[1] School of Materials Science and Engineering, YangJiang Campus, Guangdong Ocean University, Yangjiang 529500, China; [2] School of Materials Science and Engineering, Heilongjiang University of Science and Technology, Harbin 150022, China; [3] School of Materials Science and Engineering, Jiamusi University, Jiamusi 154007, China

Abstract: The impact of multi-directional compression passes on the microstructure, mechanical properties, and corrosion behavior of ZK60 magnesium alloy was investigated. Results reveal that severe dendrite segregation exists in the as-cast ZK60 magnesium alloy with coarse MgZn phases distributed along the grain boundaries. After 9 passes of compression, the coarse solidified phases at the grain boundary are significantly refined, and back dissolution occurs. Fine recrystallized grains accompanied with the fine diffused nano-phases emerge in the local area around the large grains. The tensile strength of ZK60 magnesium alloy generally exhibits the upward trend with the increase in compression passes, whereas the compression rate shows the downward trend. The compressive strength reaches 433.6 MPa with the compression rate of 21.3% after 9 passes of compression. Multi-directional compression can significantly reduce the degradation rate of ZK60 magnesium alloy in simulated body fluids. Furthermore, it is observed that in the as-cast ZK60 magnesium alloy, micro-segregation can easily lead to severe intragranular local corrosion. However, after multi-directional compression, the tendency to intragranular local corrosion is significantly diminished.

Key words: ZK60 magnesium alloy; multi-directional compression; compression passes; mechanical property; corrosion behavior

Magnesium alloys, as implant materials, exhibit excellent biocompatibility and can be degraded in the human body, becoming the frontier in biomedical materials. Nevertheless, magnesium alloy have encountered notable challenges when used for internal fracture of fixations[1–2]. Firstly, its low electrode potential leads to uncontrollable degradation rate in body fluids. Secondly, the degradation process induces significant morphological changes of the material, resulting in substantial reduction in biomechanical properties and making it difficult to meet the requirements for internal fixation[3].

Research findings indicate that both the strength and toughness of magnesium alloys can be significantly enhanced by deformation process. Furthermore, the meticulously tailored deformation process has been proven to improve the corrosion resistance of magnesium alloys[4]. However, in processes such as rolling or extrusion, metal materials require at least five independent slip systems to achieve uniform deformation. Magnesium and its alloys have the hexagonal close-packed (hcp) crystal structure, and at room temperature, only two slip systems can be activated. Consequently, the strength, ductility, and formability of this material at room temperature need to be further enhanced, severely restricting its applications[5–6]. Elevating the deformation temperature is the most commonly adopted method for magnesium alloy. With the increase in temperature, the critical resolved shear stress (CRSS) required for non-basal slip of magnesium alloy decreases significantly, whereas the CRSS for basal slip changes slightly. At 200 °C, these two values are very similar, and the magnesium alloy exhibits good plastic deformation properties, thereby enabling the plastic processing of magnesium alloy[7]. Appropriate plastic forming processes can markedly refine the grains of magnesium alloy and alter the morphology and distribution of the precipitated phases in magnesium alloy, so the deformed magnesium alloys with excellent plasticity, strength, and corrosion resistance can be widely used in various engineering fields[5–6].

Received date: February 28, 2024
Foundation item: Guangdong Ocean University Research Launch Project (060302062310)
Corresponding author: Yin Dongsong, Ph. D., Professor, School of Materials Science and Engineering, Guangdong Ocean University, Yangjiang 529500, P. R. China, E-mail: dongsongyin@gdou.edu.cn

Multi-directional compression technique, as conventional plastic deformation process, offers the advantages of easy operation, simple processing and high cost-effectiveness. Utilizing existing industrial equipment, this technique can prepare plastic deformation materials with large volume and excellent performance, thereby directly achieving large-scale industrial production[8]. Presently, research on multi-directional compression of magnesium alloys predominantly focuses on the thermal deformation behavior and micro-structural changes during compression as well as alterations of mechanical properties after compression. Typically, these studies only involve pre-annealing magnesium alloys before multi-directional compression to mitigate the adverse impact of second phase constituents on plastic deformation, facilitating substantial cumulative deformation. However, long solution treatment is required in this traditional technique, significantly increasing the preparation time of material[9].

When alloys are directly subjected to multi-directional compression without pre-solidification or softening treatments, the synergistic effect of force and heat leads to fracture and re-dissolution of the second phases, thus making early heat treatment unnecessary. This not only enhances processing efficiency but also avoids excessive grain growth caused by early heat treatment. ZK60 magnesium alloy, distinguished by excellent mechanical properties and high specific strength, is extensively used in various applications. However, research on the influence of direct multi-directional compression on the mechanical properties and corrosion resistance of ZK60 magnesium alloy is rare. Consequently, this study focused on the as-cast ZK60 magnesium alloy, which is primarily composed of Mg, Zn, and Zr, and investigated the microstructural changes and their influence on mechanical properties and corrosion resistance under varying compression passes through direct multi-directional compression. The ultimate goal is to design the processing technique for deformed ZK60 magnesium alloy, characterized by superior mechanical properties and corrosion resistance. Such insights provide significant reference for the design of multi-directional compression processes and improvement of corrosion resistance of Mg-Zn-Zr series magnesium alloys.

1 Experiment

Commercial as-cast ZK60 magnesium alloy with a chemical composition of Mg-5.20Zn-0.45Zr-0.01Fe-0.01Ni-0.01Cu (wt%) was selected as the raw material for the compression experiment. The as-cast ZK60 magnesium alloy used for the multi-directional compression experiment had dimensions of 20 mm×20 mm×17 mm, as shown in Fig.1. The high-temperature multi-directional compression experiment was conducted on the electronic universal testing machine (CMT535-300 KN) with a self-made resistance furnace. The experimental equipment is shown in Fig.2.

Upon reaching the required temperature of experiment, the furnace was opened to place the samples. After the samples were kept at the experiment temperature for 5 min, the compression experiment started. After one compression test,

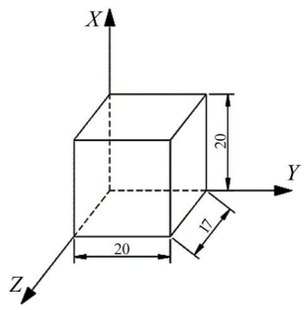

Fig.1 Schematic diagram of compression sample

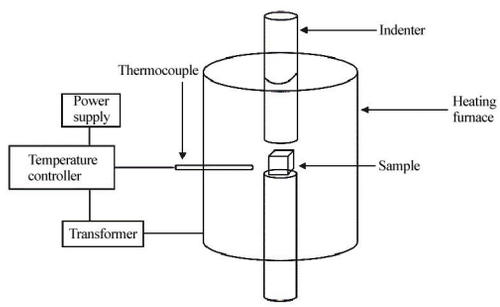

Fig.2 Schematic diagram of the thermal compression device

the sample was quenched in water. Following the compression experiment in the specific axial direction of the sample, the compression axis was rotated by 90° and the procedure was repeated for the next compression test. In this study, the compression ratio was calculated as 20% of the axial length for each compression.

After the multi-directional compression experiment, the sample was cut into two parts (Fig. 3) along the direction of load at the end of the final compression pass and the direction of downward pressure at the subsequent step of the compression cycle. One part was used to observe microstructure of the alloy, and the other part was used for performance testing. Before grinding, the sample was mechanically polished with the polishing machine. The etching liquid (5 g trinitrophenols+5 mL acetic acid+100 mL anhydrous ethanol+10 mL distilled water) was employed to corrode the samples for grain morphology observation. Dendrite morphology was corroded using 3wt% nitrate alcohol. The etching process lasted 3–5 s. The metallographic observation was conducted using Zeiss Axio Lab.A1 Zeiss optical microscope (OM).

X-ray diffraction (XRD, DX-2700B) with Cu-Kα radiation was used to characterize the phase composition of the samples before and after compression. The scanning range of the diffraction angle 2θ was 20°–100°, the scanning speed was 4°/min, and the working voltage was 30 kV. The microstructure and composition of the samples were observed by scanning electron microscope (SEM, Hitachi SU5000) and transmission electron microscope (TEM, FEI Talos F200X). The samples were mechanically thinned to thickness of 200 μm and then ion thinning was performed. The dislocation, grain, grain boundary, and second phase particles of the

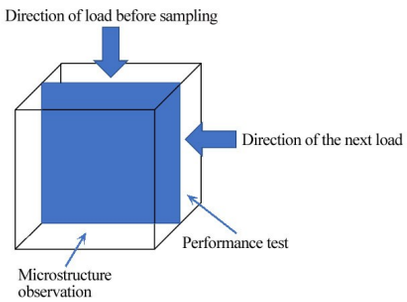

Fig.3 Schematic diagram of sampling

samples were mainly observed.

The room temperature compression test of the sample was conducted in accordance with the relevant standard of GB/T7314-2005 "Metallic materials-Compression test method at room temperature". The sample was the cylinder with diameter of 4 mm and height of 5 mm. The room temperature compression test was conducted with the test machine WDW-100A, and the compression rate was 3×10^{-3} s^{-1}.

The electrochemical test of samples was conducted on CS-350PA-type electrochemical workstation. Before the test, the surface of the sample was finely ground with 600#, 1000#, and 1200# metallographic sandpaper, followed by cleaning with deionized water and alcohol, and drying with hairdryer in cold air. The standard three-electrode system was adopted in the electrochemical experiment. The sample to be tested was the working electrode, the platinum electrode was the auxiliary electrode, and the reference electrode was saturated calomel, which was tested in Hank's solution (8.0 g/L NaCl, 0.4 g/L KCl, 0.06 g/L Na_2HPO_4, 0.06 g/L KH_2PO_4, 0.35 g/L $NaHCO_3$, 0.2 g/L $MgSO_4\cdot7H_2O$, 0.14 g/L $CaCl_2$). Firstly, the sample was immersed in Hank's solution for the open-circuit potential (OCP) test. After OCP value of the sample was stabilized, the electrochemical impedance spectroscopy (EIS) test was conducted. The scanning frequency of the test was 10^{-1} – 10^{5} Hz, and the amplitude of alternating current was 10 mV. Finally, the potential range of the potential polarization test was OCP±0.5 V, and the scanning speed was 1 mV/s. The self-corrosion potential (E_{corr}) and self-corrosion current density (I_{corr}) of the samples were obtained by the cathodic linear partial extrapolation of the Tafel curve. To ensure the reliability of the experimental outcomes, three samples were prepared for each processing technique and tested many times.

The solution used for immersion experiment contained the same composition as that used for the electrochemical experiment, which was Hank ' s solution. To create the immersion environment that closely matched the real human body environment, the thermostatic water bath was used to maintain the temperature of the immersion solution at 37 °C. The solution was replaced every 24 h during the experiment. The ratio of the exposed surface area of the test sample to the volume of simulated body fluid was 1 cm^2:30 mL.

The sample used for the immersion experiment was a cube of 3 mm×7 mm×9 mm, and the six surfaces of the cube were finely ground with 2000# metallography sandpaper. After immersion, the sample was ultrasonically cleaned for 10 min with the mixture of 200 $g\cdot L^{-1}$ CrO_3 +10 $g\cdot L^{-1}$ $AgNO_3$ in boiling water to remove the corrosion products on the sample surface. After drying, the mass of the sample after immersion was recorded. Three immersion samples were prepared for each processing technique and repetitive experiments were conducted to improve the accuracy of experimental results.

The corrosion rate of the alloy is calculated, as follows:

$$CR = \frac{8.76 \times 10^4 \times \Delta W}{ATD} \quad (1)$$

where CR is the average mass loss corrosion rate (mm/a), ΔW is the mass difference of the sample before and after immersion test (g), A is the surface area of the sample exposed to the solution (cm^2), T is the immersion time (h), and D is the alloy density (1.74 g/cm^2).

2 Results and Discussion

2.1 Microstructure

Fig. 4 shows the microstructure of ZK60 alloy before and after multi-directional compression deformation with different passes. The grain size of the alloy decreases with the increase in compression passes. When the multi-directional compression reaches 9 passes (Fig.4d), the grain size of the alloy is the smallest. The same conclusion can be found through the average grain size of the alloy, as shown in Fig. 5. Upon comparing the microstructure after 6 passes, it is evident that the grains of alloy undergo further fragmentation and refinement. Notably, in regions A and B of Fig. 4d, the cumulative increase in compressive deformation leads to the generation of fine recrystallized grains around the large grains. This change results in the decrease in the homogenization degree of alloy after 9 passes of compression, compared with that after 6 passes of compression.

The phenomenon of dynamic recrystallization in metal can only occur when the critical deformation amount is reached, and the deformation temperature is higher. At the compression temperature of 350 °C, the substantial deformation of ZK60 magnesium alloy is achieved with the increase in deformation passes. Numerous deformation defects such as dislocations and subgrain boundaries are introduced into the deformed magnesium alloy matrix, which can be eliminated through the nucleation and grain growth of dynamic recrystallization. The primary mechanism can be explained as follows. After large plastic deformation, numerous high-density dislocation regions are formed in the alloy, leading to local migration of grain boundaries and the formation of bumps[10]. The slip of non-planar grain boundary induces strong strain gradient around the grain boundary[11–12]. Dislocation sources located at grain boundaries emit dislocations into grains to coordinate plastic deformation, which generally belong to non-basal systems. The dislocations of the non-basal system interact with dislocations of basal plane to form subgrain boundaries, cutting off the protruding part of the original grain. With the

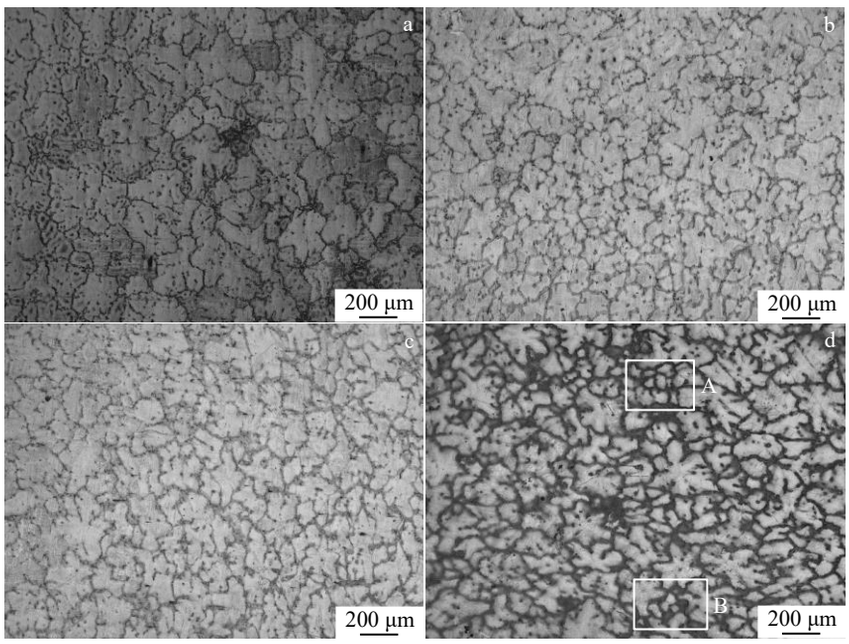

Fig.4 OM images of ZK60 magnesium alloy at different states: (a) as-cast; (b) 3 passes; (c) 6 passes; (d) 9 passes

continuous accumulation of strain, new lattice dislocations are added to the subgrain boundaries, resulting in the increase in the orientation difference of subgrain boundaries and eventually developing into the large-angle grain boundary.

Fig. 6 presents SEM images of as-cast ZK60 magnesium alloy before and after multi-directional compression. There are stripy, blocky, and elliptical bright white phases distributed on the gray magnesium alloy matrix. The stripy phases are situated at the grain boundaries and the elliptical phases are within the crystals. This microstructure is characteristic of the solidification microstructure of Mg-Zn alloy[13].

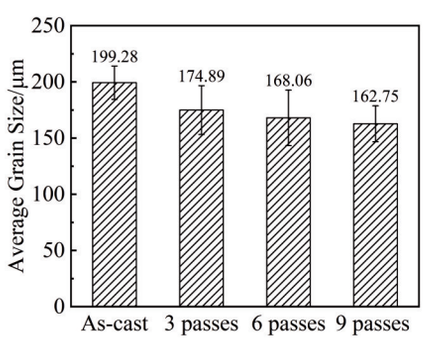

Fig.5 Average grain sizes of ZK60 magnesium alloys at different states

After 3 passes of multi-directional compressions (Fig. 6b), the size and quantity of the stripy phases at the grain boundaries and the elliptical phases within the crystals are significantly reduced. With the further increase in compression passes to 9 (Fig. 6c), a substantial number of grain boundary phases are transformed into granular phases, and the elliptical phases nearly disappear.

XRD patterns of as-cast ZK60 magnesium alloy before and after multidirectional compression are shown in Fig. 7. Following multi-directional compression, the phase composition of the alloy remains unchanged, primarily consisting of three phases: α-Mg, MgZn and $MgZn_2$. These detailed observations provide valuable insights into the structural changes of ZK60 magnesium alloy after multi-directional compression and the stability of its phase composition during the deformation process.

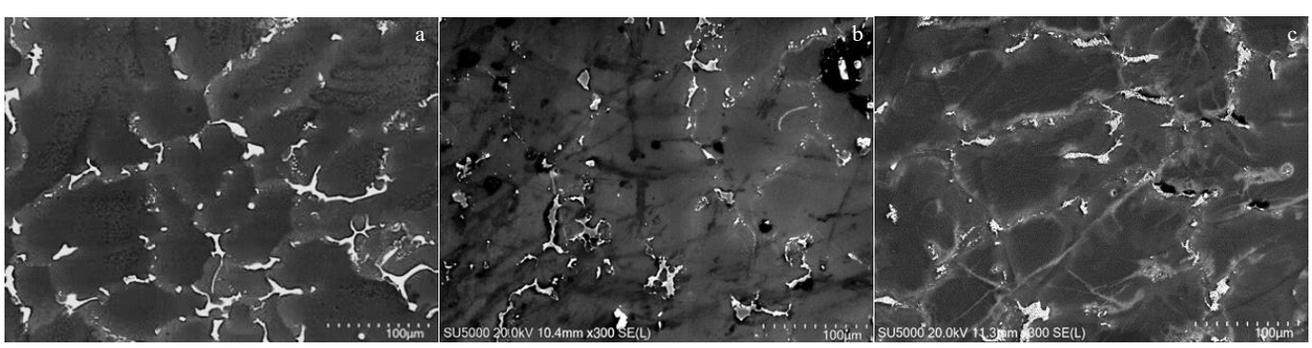

Fig.6 SEM images of ZK60 magnesium alloy at different states: (a) as-cast; (b) 3 passes; (c) 9 passes

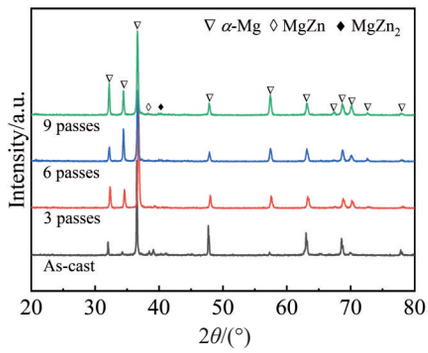

Fig.7 XRD patterns of ZK60 magnesium alloy at different states

Fig. 8 illustrates TEM images of the as-cast ZK60 magnesium alloy after 9 passes of multi-directional compression deformations. In Fig. 8a, numerous dislocations are observed in the magnesium alloy matrix. Fig. 8b reveals the generation of dynamic recrystallization grains with the size of approximately 500 nm around the large deformed grains. There are extremely fine nano-phase particles distributed around the recrystallized grains. The process of grain boundary energy storage and stress promotes the precipitation of the second phases at the grain boundary.

In Fig. 8c, the secondphase particles and the α-Mg matrix can be observed. EDS results of spot 1 and 2 in Fig. 8c are listed in Table 1, indicating that both spots are composed of Mg and Zn elements, with no presence of Zr element. These detailed observations provide valuable insights into the microstructural changes, dislocation formation, and dynamic recrystallization of the ZK60 magnesium alloy after extensive multi-directional compression, shedding light on its mechanical behavior and potential applications in structural materials.

Fig.9 shows TEM image and EDS mappings of ZK60 alloy after 9 passes of multi-directional compression. EDS mappings show that Zn element is concentrated at the grain boundaries and only present in small amount in the crystals. The content of Zn element in the α-Mg matrix is relatively low. The distribution of Zr element in the alloy is the same as that of Zn element, and it in the second phase is closely related with that in α-Mg matrix. It can be inferred that after extensive deformation of the ZK60 magnesium alloy, the Mg-Zn phases undergo fragmentation and dissolution, thereby increasing the solid solubility of Zn element in the α-Mg matrix. Induced by significant deformation storage energy and stress, both the MgZn and ZnZr phases are precipitated at the grain boundaries[14]. These findings offer valuable insights into the elemental distribution and contribute to understanding of the deformation-induced changes in composition and structure of the ZK60 magnesium alloy during multi-directional compression.

2.2 Compression performance

Fig. 10 presents the engineering stress-engineering strain curves of as-cast ZK60 magnesium alloy before and after different passes multi-directional compression deformation. The corresponding mechanical properties are detailed in Table 2. Compared with the as-cast ZK60 magnesium alloy, the yield strength of ZK60 alloy after 3 passes of compression remains relatively unchanged, while the yield strength and compressive strength of ZK60 alloy are significantly improved with the increase in compression passes from 6 to 9. Specifically, compared with those of as-cast ZK60 magnesium alloy, the yield strength of ZK60 alloy after 9 passes of compression increases from 131.5 MPa to the peak of 199.1 MPa, and the compressive strength rises from 372.9 MPa to 433.7 MPa.

The accumulation of substantial strain during multi-pass and multi-directional deformation refines the microstructure of the alloy. External compression results in refined grains, signifying the presence of more grain boundaries that impede

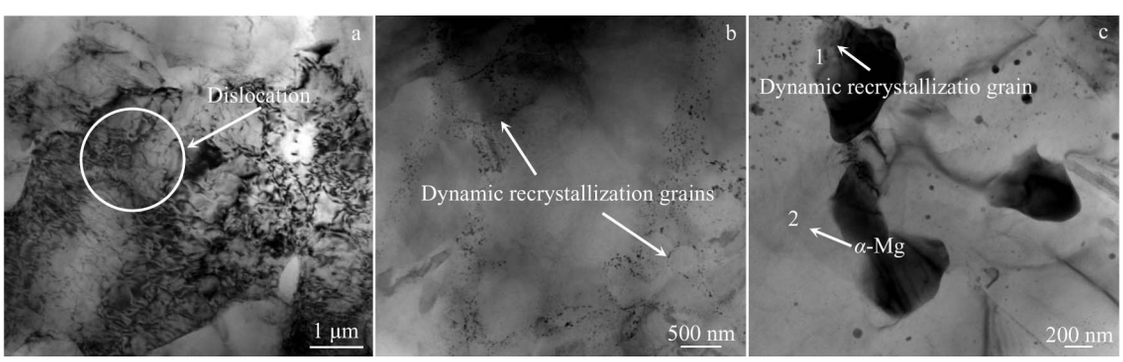

Fig.8 TEM images of ZK60 alloy after 9 passes of multi-directional compression: (a) dislocation; (b–c) dynamic recrystallization grains and dispersion of precipitates

crack expansion. Moreover, multi-directional compression and the fine dispersed solidification precipitates contribute to the dispersion strengthening effect. Notably, the grain boundary and the precipitated fine dispersed nano-phase (Fig. 9) impede grain boundary slip, thereby enhancing the compressive

Table 1 EDS results of spots marked in Fig.8c (wt%)

Spot	Mg	Zn
1	50.37	49.62
2	94.71	5.29

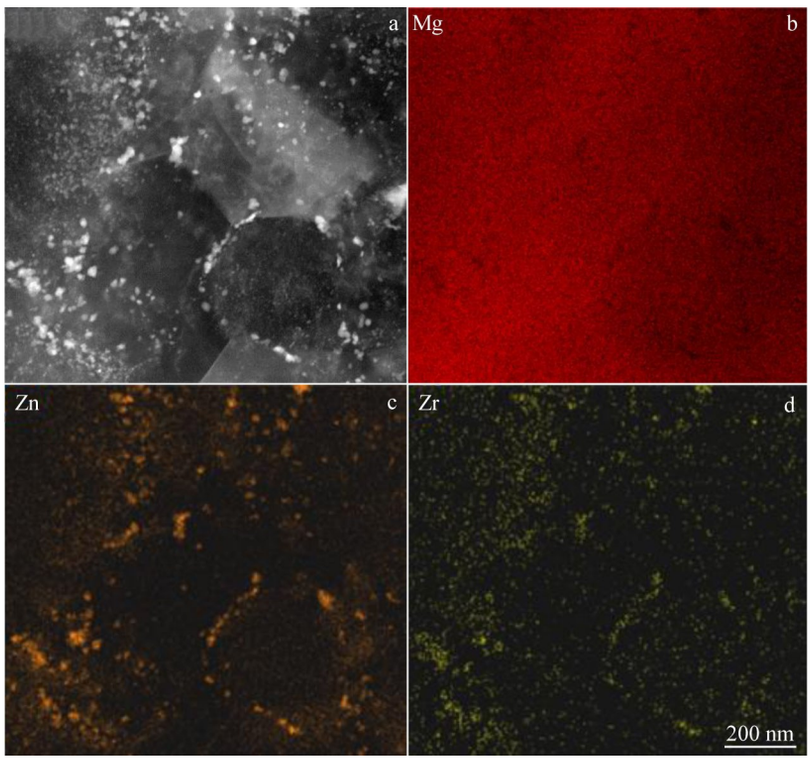

Fig.9 TEM image (a) and EDS element mappings (b–d) of ZK60 alloy after 9 passes of multi-directional compression: (b) Mg, (c) Zn, and (d) Zr

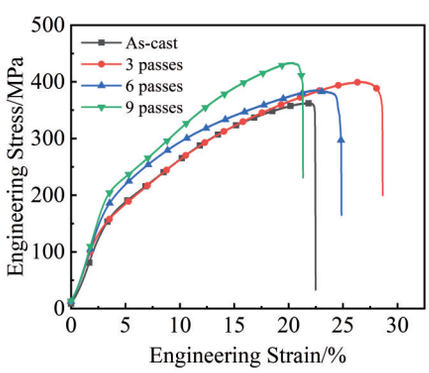

Fig.10 Engineering stress-engineering strain curves of ZK60 magnesium alloys at different states

Table 2 Mechanical properties of ZK60 magnesium alloys in different states

State	Yield strength/MPa	Compressive strength/MPa	Elongation/%
As-cast	131.5±1.1	372.9±2.1	23.5±2.3
3 passes	134.7±2.3	399.1±1.6	27.6±1.7
6 passes	173.5±2.9	387.0±2.6	25.1±1.6
9 passes	199.1±2.1	433.7±1.6	20.6±2.1

strength and yield strength[15–16]. The matrix of ZK60 magnesium alloy with 9 passes of multi-directional compression has a large number of dislocations, further enhancing the strength of alloy. When the alloy is subjected to external stress, the atoms in the alloy will try to ease the stress by sliding. But the existence of dislocation clusters will hinder the sliding of the atoms, resulting in local stress concentration, which will reduce the compression rate of the alloy.

2.3 Corrosion behavior

The polarization curves of as-cast ZK60 magnesium alloy before and after different passes of multi-directional compression are depicted in Fig. 11, and the fitting results are listed in Table 3. The comparison with the corrosion properties of original as-cast ZK60 magnesium alloy reveals that the absolute value of self-corrosion potential of the deformed alloy is decreased. When the deformation pass of multi-directional compression gradually increases from 3 to 9, the absolute value of self-corrosion potential

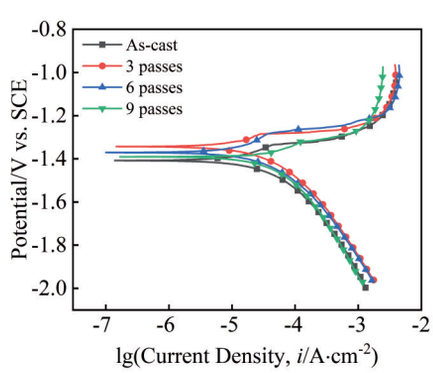

Fig.11 Polarization curves of ZK60 magnesium alloys at different states

Table 3 Electrochemical parameters obtained from the polarization curves of ZK60 magnesium alloys at different states

State	Self-corrosion potential, E_{corr}/V vs. SCE	Self-corrosion current density, i_{corr}/μA·cm^{-2}
As-cast	−1.3924	53.59
3 passes	−1.3317	25.40
6 passes	−1.3532	36.78
9 passes	−1.3869	38.34

is gradually increased. The self-corrosion current density of the alloy decreases significantly from 53.59 μA·cm^{-2} to 25.40 μA·cm^{-2} with the increase in compression pass from 0 to 3. As the number of multi-directional compression passes increases to 6, the self-corrosion current density rises to 36.78 μA·cm^{-2}, and with the further increase to 9 passes of compression, the self-corrosion current density continues to rise.

These findings highlight the influence of multi-pass compression deformation on the corrosion behavior of ZK60 magnesium alloy. The increasing absolute value of self-corrosion potential and the decreasing self-corrosion current density suggest that corrosion resistance is improved with the increase in compression passes, providing valuable insights for the development of corrosion-resistant magnesium alloys for various applications.

Fig. 12 illustrates the corrosion rate of as-cast ZK60 magnesium alloy before and after different passes of multi-directional compression in simulated body fluid. The

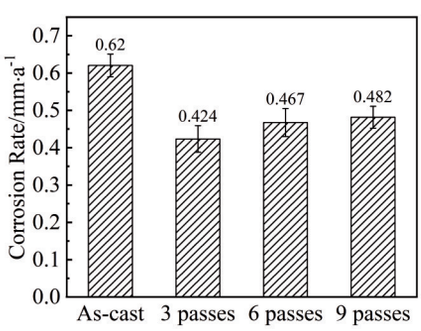

Fig.12 Corrosion rates of ZK60 magnesium alloys at different states

immersion experiment lasted for 7 d with Hank's solution as the immersion medium. Compared with the as-cast magnesium alloy, it is evident that the corrosion rate of the alloy after large deformation processes is significantly decreased. When the number of multi-directional compression passes is 3, the minimum corrosion rate of ZK60 alloy is 0.424 mm/a. Notably, there is no significant difference in corrosion rate between the sample after 6 passes and that after 9 passes. However, the corrosion rate of the sample after 6 compression passes is slightly smaller as 0.467 mm/a.

These results underscore the impact of multi-directional compression deformation on the corrosion behavior of ZK60 magnesium alloy in simulated body fluid. The marginal decrease in corrosion rate of the alloy after 6 compression passes indicates that corrosion resistance is enhanced, providing valuable insights for the development of corrosion-resistant magnesium alloys for biomedical applications.

The morphologies of the as-cast ZK60 magnesium alloy after corrosion in simulated body fluid are shown in Fig.13. It is evident that the as-cast alloy undergoes severe corrosion in the simulated body fluid. The corrosion sites exhibit distinct characteristics. The part with light corrosion shows the similar shape to dendrite (zone A in Fig. 13a). Analysis suggests that these regions represent the α -Mg leading phase in the early stages of solidification, characterized by non-equilibrium solidification. As dendrites grow, solute redistribution occurs, leading to Zn element enrichment at the advancing front of the solid-liquid interface. Consequently, Zn element is concentrated in the edge of the dendrite arm, whereas the Zn content in the central region of the dendrite arm is relatively low[17–18]. This phenomenon results in lower corrosion resistance of the dendrite arm compared with that at the dendrite edge, giving rise to corrosion along the dendrite arm. This corrosion deepens progressively, as illustrated in zone B of Fig. 13a, and continues to expand and coalesce, ultimately culminating in more severe corrosion, as depicted in zone C of Fig. 13a and zone D of Fig. 13b. EDS results of the corrosion bulge (point 1 in Fig. 13c) and corrosion depression (point 2 in Fig. 13c) are presented in Table 4. The findings reveal that the Zn content at point 1 is significantly higher than that at point 2,

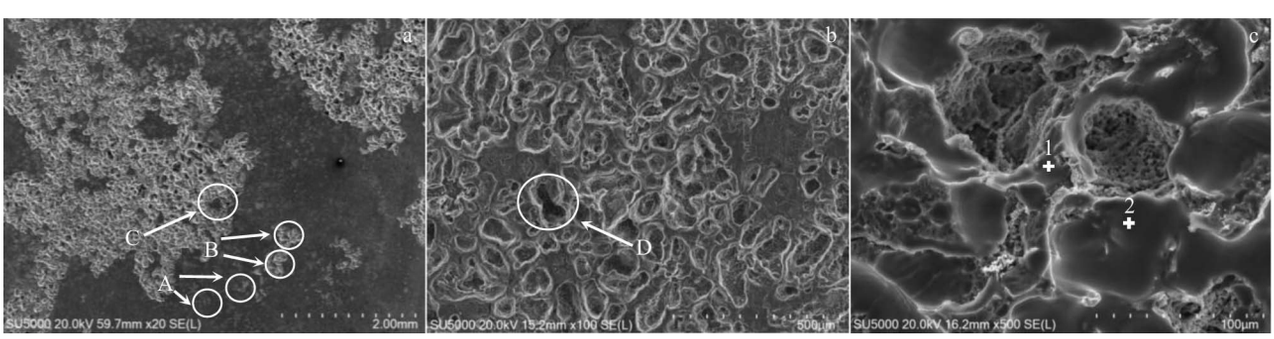

Fig.13 Corrosion morphologies of as-cast ZK60 magnesium alloys after removing corrosion products

corroborating the aforementioned analysis. Based on this analysis, the corrosion process diagram of as-cast ZK60 magnesium alloy is established in Fig.14.

Fig. 15 shows corrosion morphologies of as-cast ZK60 magnesium alloys at different states. Evident alterations are observed in the corrosion morphologies of ZK60 magnesium alloy after 3 passes of multi-directional compression, as illustrated in Fig. 15a and 15b. The corrosion pits are significantly reduced in number and become shallower. After 3 passes of multi-directional compression, dendritic corrosion appears even in areas with mild corrosion, resulting in the milder dendrite zone and shallower smaller corrosion grooves (zone A in Fig.15a and zone D in Fig.15b). The development and deepening of this corrosion are apparently shown in zone B and zone C of Fig.15a. The resultant corrosion pits expand and connect in zone C of Fig. 15a and zone F of Fig. 15b, which are different from the corrosion pits observed in the as-cast alloy.

Table 4 EDS results of points marked in Fig.13c (wt%)

Point	Mg	Zn	Zr
1	94.47	5.53	0.00
2	95.01	3.61	1.38

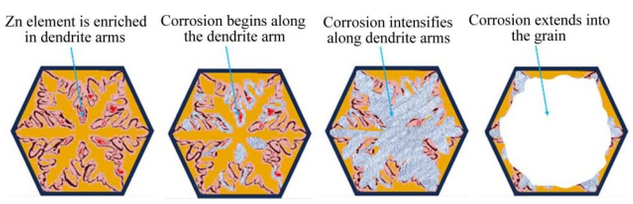

Fig.14 Schematic diagrams of corrosion process of as-cast ZK60 magnesium alloy

After 6 and 9 passes of multi-directional compressions, the morphologies of ZK60 magnesium alloy are depicted in Fig. 15c – Fig. 15f. It is clear that the corrosion morphologies of ZK60 magnesium alloy after 6 and 9 passes of multi-directional compression remain similar to that after 3 passes, but their number and size of corrosion pits significantly increase, compared with those after 3 passes of multi-directional compression. The dendrites exhibit numerous deep and severe local corrosion behavior (zone G in Fig. 15d). Additionally, ZK60 alloy subjected to 9 passes of multi-directional compression also displays the closed annular corrosion in local region (zone H in Fig. 15f) with similarly dispersed recrystallization phase in the corrosion center.

In conclusion, it is evident that for the ZK60 magnesium alloy, the corrosion resistance exhibits the trend of initial enhancement followed by decrease with the increase in multi-directional compression passes, although it generally surpasses that of the as-cast alloy. This phenomenon is attributed to the presence of dendrite segregation in the ZK60 magnesium alloy and the enrichment of Zn element at the edges of the dendrite arms. Furthermore, solidification precipitates with various sizes and shapes are present in the grain boundaries and intracrystalline dendrites, and the electrode potential in these regions is higher than that of the dendrite arms, leading to micro-galvanic corrosion. Initially, dendrite corrosion occurs, as shown in Fig.15b. For the as-cast alloy, corrosion continues to expand with the prolongation of immersion time. Ultimately, micro-galvanic corrosion forms between the solidification phase at the grain boundary and the crystal, resulting in severe corrosion within the crystal and the formation of holes.

After 3 passes of multi-directional compression, the structure of as-cast alloy undergoes significant changes due to

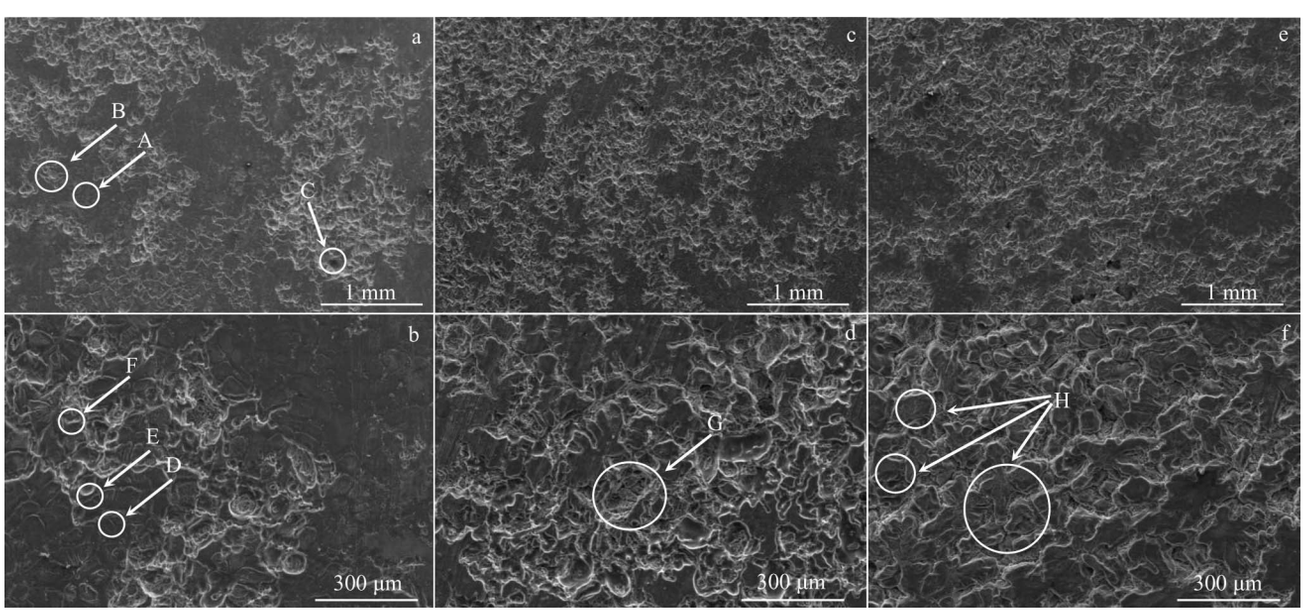

Fig.15 Corrosion morphologies of as-cast ZK60 magnesium alloys at different states after removing corrosion products: (a–b) 3 passes; (c–d) 6 passes; (e–f) 9 passes

the combined influence of heat and forces of multi-directional compression. Initially, the solidified precipitates break and redissolve. Concurrently, Zn atoms diffuse from high to low concentration zones, leading to the substantial reduction in dendrite segregation[19]. These alterations result in the decrease in the number of cathode phases, the decrease in the self-corrosion current density in the anode region (Table 3), and the notable reduction in corrosion rate (Fig. 12), thereby enhancing the uniformity and stability of the matrix. After 6 passes of multi-directional compression, the quantity, size, and dendrite segregation of solidification phases continue to decrease. However, with the increase in deformation, the number of vacancies, dislocations, and substructures in the alloy matrix rises, generating new anode regions with diminished corrosion resistance (Fig. 15a – 15b), and subsequently leading to the increase in self-corrosion current density (Table 3). After 9 passes of multi-directional compression, the number and size of solidified phases are significantly decreased, accompanied by the appearance of small recrystallized grains in local regions. Furthermore, there are abundance of dislocations in the crystal (Fig.8) and widely precipitated dispersed phases at the grain boundary (Fig. 8). These phenomena contribute to the increase in the number of anode and cathode regions. Additionally, the coarse grain region exhibits the higher initial electrode potential, whereas the fine grain region displays lower initial electrode potentials. Consequently, anode regions are formed during corrosion, causing more severe corrosion of the alloy in these regions[20]. The cumulative impact of these factors leads to the continuous increase in the corrosion current of the alloy, subsequently escalating the corrosion rate and slightly diminishing corrosion resistance.

3 Conclusions

1) The dendrite segregation of ZK60 alloy is reduced after multi-pass and multi-directional compression. After 9 passes of multi-directional compression, recrystallized grains appear around the large grains, and there are fine dispersed nano-phase precipitation around the grains.

2) The compressive strength of ZK60 magnesium alloy exhibits substantial increase with the increase in compression passes. With 9 passes of compression, the yield strength of ZK60 alloy rises from 131.5 MPa to 199.1 MPa, and the compressive strength increases from 372.9 MPa to 433.7 MPa.

3) After multi-directional compression, the local corrosion tendency of ZK60 alloy is reduced, and the average corrosion rate of ZK60 alloy is the lowest of 0.424 mm/a after 3 passes of compression.

References

1 Niranjan C A, Raghavendra T, Rao M P *et al. Journal of Magnesium and Alloys*[J], 2023, 11(8): 2688

2 Bakhshenshi-Rad H R, Idris M H, Abdul-Kadir M R *et al. Materials and Design*[J], 2013, 53: 283

3 Tang H, Wu T, Wang H *et al. Journal of Alloys and Compounds*[J], 2017, 698: 643

4 Guo Qiang, Yan Hongge, Chen Zhenhua *et al. Transactions of Nonferrous Metals Society of China*[J], 2006, 16(4): 922

5 Guo Weimin, Li Nan, Zhou Jixue *et al. Metallography, Microstructure, and Analysis*[J], 2021, 10(1): 46

6 Li Jianping, Xia Xiangsheng. *Journal of Materials Engineering & Performance*[J], 2015, 24(9): 3539

7 Koike J, Kobayashi T, Mukai T *et al. Acta Materialia*[J], 2003, 51(7): 2055

8 Sitdikov O, Goloborodko A, Sakai T *et al. Materials Science Forum*[J], 2003, 426–432(1): 381

9 Chen Q, Zhao Z X, Shu D Y *et al. Materials Science & Engineering A*[J], 2011, 528(10): 3930

10 Liu Chuming, Liu Zijuan, Zhu Xiurong *et al. The Chinese Journal of Nonferrous Metals*[J], 2006, 16(1): 1 (in Chinese)

11 Belyakov A, Miura H, Sakai T. *Materials Science and Engineering A*[J], 1998, 255(1–2): 139

12 Miura H, Aoyama H, Sakai T. *Journal of the Japan Institute of Metals*[J], 1994, 58(3): 267

13 Peng Peng, Zhang Kunmin, She Jia *et al. Journal of Alloys and Compounds*[J], 2021, 861: 157958

14 Verissimo N C, Brito C, Santos W L R *et al*. *Journal of Alloys and Compounds*[J], 2016, 662: 1

15 Jamali A, Mahmudi R. *Materials Science & Engineering A*[J], 2023, 884: 145552

16 Wang Yuye, Zhou Haitao, Li Yi *et al*. *The Chinese Journal of Nonferrous Metals*[J], 2024, 34(3): 683 (in Chinese)

17 Chen Weipeng, Hou Hua, Zhang Yuntao *et al. Journal of Materials Research and Technology*[J], 2023, 24: 8401

18 Du Jinglian, Guo Zhipeng, Yang Manhong *et al. Materials Today Communications*[J], 2017, 13: 155

19 Li Zhen, Peng Zeyin, Qiu Yubing *et al. Journal of Materials Research and Technology*[J], 2020, 9(5): 11201

20 Zeng R C, Kainer K U, Blawert C *et al. Journal of Alloys and Compounds*[J], 2011, 509(13): 4462

压缩道次对ZK60镁合金力学性能和腐蚀行为影响

尹冬松[1]，刘志远[2]，张游游[2]，毛　勇[2]，韩天明[3]

(1. 广东海洋大学(阳江校区) 材料科学与工程学院，广东 阳江 529500)

(2. 黑龙江科技大学 材料科学与工程学院，黑龙江 哈尔滨 150022)

(3. 佳木斯大学 材料科学与工程学院，黑龙江 佳木斯 154007)

摘　要：研究了多向压缩道次对ZK60镁合金组织、力学性能和腐蚀行为的影响。结果表明，铸态ZK60镁合金枝晶偏析较为严重，晶界处分布着粗大的MgZn相。当压缩道次增加到9道次时，晶界处的粗大凝固相显著细化，并发生回溶，大晶粒周围的局部区域出现细小的再结晶晶粒，并在再结晶晶粒周围析出细小弥散的纳米相。随着压缩道次的增加，ZK60镁合金的抗拉伸强度总体呈上升趋势，压缩率呈下降趋势，9道次时抗压强度为433.6 MPa，压缩率为21.3%。多向压缩可显著降低ZK60镁合金在模拟体液中的降解率，对于铸态ZK60镁合金，微观偏析容易导致严重的晶内局部腐蚀，但是经过多向压缩后，晶内局部腐蚀倾向明显减弱。

关键词：ZK60镁合金；多向压缩；压缩道次；力学性能；腐蚀行为

作者简介：尹冬松，男，1974年生，博士，教授，广东海洋大学（阳江校区）材料科学与工程学院，广东 阳江 529500，电话：0662-2162025，E-mail：dongsongyin@gdou.edu.cn